ACS OMEGA

Open Access

http://pubs.acs.org/journal/acsodf

Article

A Levodopa-Encapsulated Poly-ε-Caprolactone Nanocomposite Improves the Motor Symptoms and Neurochemical Changes in a Rotenone-Induced Mouse Model of Parkinson's Disease

Ramesha Hanumanthappa, Geetha B. Heggannavar, Aishwarya Banakar, Divya D. Achari, Vijaykumar Ramesh Karoshi, B. R. Radha Krushna, Asmatanzeem Bepari, Rasha Assad Assiri, Hanan Nasser Altamimi, Hemalatha Nanjaiah, Devaraja Sannaningaiah, Shamprasad Varija Raghu, Vishwas Kaveeshwar, H. Nagabhushana, and Kuramkote Shivanna Devaraju*

Cite This: *ACS Omega* 2025, 10, 19682−19696

Read Online

ACCESS | Metrics & More | Article Recommendations | Supporting Information

ABSTRACT: Parkinson's disease (PD) is the most common neurodegenerative disorder; in this condition, patients lose dopamine (DA), which leads to abnormal motor functions. Levodopa (LD) is the most effective drug used for the treatment of PD; however, LD shows poor plasma bioavailability and limited brain uptake and induces peripheral side effects. Due to its poor brain availability and short half-life, prolonged treatment must be repeated with a dosing schedule, which leads to long-term side effects, including dyskinesia, stomatitis, anxiety, and depression. An LD-encapsulated polymer nanocomposite has been reported to overcome these problems. The present study aims to improve the bioavailability and efficiency of LD to an effective treatment strategy for PD. Herein, we report the newly synthesized LD-encapsulated poly-ε-caprolactone (PCL) nanocomposite (LD-PCL-PVA NC), and its chemical and physical properties were analyzed. The LD-PCL-PVA NC exhibits no toxicity on the SH-SY5Y cell line and shows improved bioavailability of the LD in mouse plasma. Furthermore, we found that LD-PCL-PVA NC showed a significant improvement in motor symptoms in the rotenone (RT)-induced PD mouse model compared to the LD treatment. In addition, LD-PCL-PVA NC significantly increased the DA and homovanillic acid compared to LD and restored the total glutathione level and malonaldehyde and catalase activity in mouse brain. The histopathology studies reveal that LD-PCL-PVA NC did not exhibit toxicity in treated mice. The study suggested that LD-PCL-PVA NC can be used for the effective and promising treatment of PD.

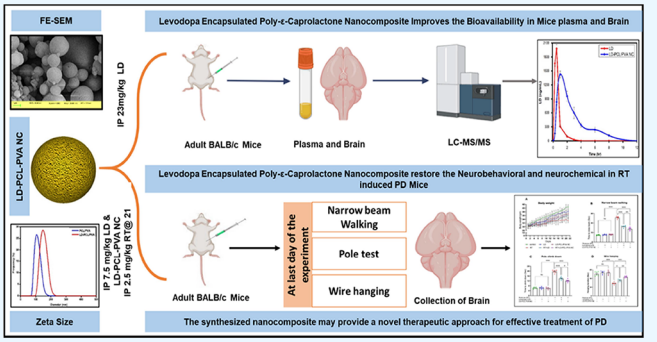

INTRODUCTION

Parkinson's disease (PD) is the most common age and movement-related progressive neurodegenerative disorder.[1] 0.2% of the global population is suffering from PD, including 1% of those above 60 years and 4% of those above 80 years.[2] The unique feature of this condition is a decreased level of dopamine (DA), due to the progressive loss of dopaminergic neurons (DPN) in the substantia nigra, pars compacta of the midbrain.[3] In this condition, patients begin to notice symptoms such as stiffness of limbs and muscles, tremors, bradykinesia, impaired walking, and coordination.[4] Yet, the exact causes of PD are unknown but are believed to be influenced by the accumulation and aggregation of an α-synuclein protein called Lewy bodies by the mutation of the Synuclein Alpha (SNCA) gene.[5] However, these mutations account for only a small proportion of the PD cases. The exact mechanisms behind sporadic alpha-synuclein aggregation are still under investigation, but previous research suggests that oxidative stress, mitochondrial dysfunction, and neuroinflammation are thought to play a significant role.[6] Lewy bodies further aggregate in the mitochondria, which leads to the generation of reactive oxygen species (ROS) and neuroinflammation, which damage the nigral cells. There are many medications, such as Ropinirole,[7] Pramipexole,[8] Levodopa,[9] Benztropine, Rotigotine, and Apomorphine,[10] that can be used to treat the different symptoms of PD, but none have been effective in preventing or terminating the PD symptoms completely.

Received: January 22, 2025
Revised: April 10, 2025
Accepted: April 25, 2025
Published: May 6, 2025

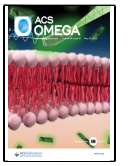

In the 1960s, Levodopa (LD) or l-3,4-dihydroxyphenylalanine, the precursor of DA, was developed to treat PD, and it continues to be the most effective therapeutic agent for PD.[11] However, only one percent of the administered LD can reach the brain due to its short half-life and poor pharmacokinetic properties.[12] Furthermore, the hydrophilic compound of LD is degraded by enzymes in the gastrointestinal tract, and it is decarboxylated by DOPA decarboxylase during the first pass of hepatic metabolism and systemic circulation, leading to a short half-life period.[9] The half-life and long-time treatment of LD leads to multiple side effects, including dyskinesia,[13] sleep disturbance, anxiety,[14] etc. The carbidopa is coadministered to prevent the rapid metabolism of LD, but this combination of drugs causes leg pain, ataxia, and increased tremors.[15] For this reason, modifications of available drugs, improvements of existing drugs, and the synthesis of novel drugs are necessary for the effective treatment of PD.

To overcome these problems, united with LD therapeutics, especially bioavailability and biodistribution, polymer-based nanoparticles have attracted a lot of attention recently across the world.[6,16,17] In this context, the study focused on the development of polymer-based drug-encapsulated nanocomposites (PDENCs) to increase drug bioavailability and biodistribution. LD-encapsulated polymeric nanoparticles have increased the blood−brain barrier crossing and maintained prolonged release without peripheral metabolism, thereby reducing the repeated drug administration.[12,18] While keeping these advantages in mind, we synthesized an LD-encapsulated poly-ε-caprolactone (PCL) nanocomposite (LD-PCL-PVA NC) to increase the bioavailability and sustained release. Compared to all polymers, the semicrystalline synthetic PCL has some unique features such as biodegradability, biocompatibility, thermal stability, nontoxicity, and high encapsulation capacity.[19] The PCL polymer is biodegradable due to the presence of an ester group. These ester groups undergo degradation through hydrolysis in chemical or enzymatic pathways.[20] The Food and Drug Administration (FDA) has approved the PCL polymer for human use and cell therapies in specific applications.[21] As per previously reported research, Carboplatin,[22] Doxorubicin,[23] Paclitaxel,[24,25] Doxycycline,[26] Leflunomide,[27] Lamotrigine,[28] Aripiprazole,[29] Rivastigmine,[30] 5-fluorouracil,[31] Etoposide, and Carmustine[32] drugs are encapsulated in PCL nanoparticles and used to improve the treatment strategy of various disorders such as Alzheimer's, Schizophrenia, and various cancers.

Poly(vinyl alcohol) (PVA) is a synthetic polymer known for its exceptional chemical and physical properties. Its water-processability, biocompatibility, hydrophilicity, biodegradability, and chemical resistance, as well as the mechanical strength and flexibility of its composites, make PVA highly suitable for biomedical applications.[33] Previous studies have shown that PCL-PVA composites have been used in tissue engineering, ophthalmology, wound healing, and drug delivery.[34] The study by Kayan and Kayan proposed that the PVA-PCL biodegradable composite is more environmentally sustainable than nonbiodegradable materials.[35] Afzal et al. previously reported that the hydrophilic properties of PVA facilitate sustained and controlled drug release from the PCL matrix.[36] The combination of PCL-PVA enhances the structural integrity and water absorption capacity, which makes it beneficial for drug delivery systems and wound dressing applications. In addition, it acts as an emulsifier in nanoparticle synthesis by stabilizing the mixture and preventing particle aggregation.[37]

In the current study, we have synthesized an LD encapsulated poly-ε-caprolactone nanocomposite (LD-PCL-PVA NC) and characterized it using various techniques such as zeta size and potential, Fourier-transform infrared spectroscopy (FTIR), field-emission scanning electron microscopy (FE-SEM), and high-resolution transmission electron microscopy (HR-TEM). Furthermore, it was tested for potential bioavailability in mouse plasma and brain. Additionally, its effect was determined in restoring neurobehavioral and neurochemical secretions in the rotenone-induced Parkinson's mouse model. It was found that LD-PCL-PVA NC improved the pharmacokinetic properties and biodistribution. The LD-PCL-PVA NC also improves neurobehavior and neurochemicals in rotenone-induced PD mouse models. Furthermore, it was observed that the synthesized LD-PCL-PVA NC has no detrimental brain or vital organ toxicity. Hence, LD-PCL-PVA NC can be used to improve the biodistribution of LD and improve the treatment strategy for PD.

RESULTS AND DISCUSSION

Synthesis and Characterization of NC. Over the last few decades, nanotechnology-based medicines have gained significant attention in neurotherapeutics due to their unique properties, such as biodegradability, biocompatibility, and targeted drug release.[38,39] In this study, PCL was chosen as the polymer matrix for LD formulation, as previous research demonstrated its effectiveness in encapsulating drugs like Paclitaxel,[25] Doxorubicin,[23] Doxycycline,[26] and Leflunomide[28] for treating neurological disorders.

In the synthesis of LD-PCL-PVA NC, initially, PCL was modified into PCL-COO$^-$, by a mild hydrolysis process with a sodium hydroxide (NaOH) solution to expose the carboxyl and hydroxyl groups in PCL (Scheme 1). The synthesis of LD-

Scheme 1. Schematic Representation of Modification of PCL to PCL-COO$^-$ Using NaOH

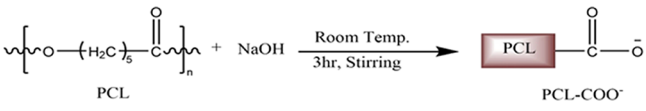

PCL-PVA NC was carried out using a double emulsion solvent evaporation method and the EDC and NHS were used for LD cross-linking with the PCL-COO$^-$[21] (Scheme 2). EDC and NHS play crucial roles in creating stable covalent bonds between LD and functional groups in PCL-COO$^-$. In the final step, LD-PCL was emulsified with PVA to stabilize NC formation, resulting in the formation of NC that is dispersible in aqueous media (Scheme 2).

The Z average size and polydispersive index (PDI) of the synthesized NC were determined by the dynamic light scattering (DLS) technique and the resulting data are shown in Figure 1A. The data revealed that the average sizes of the PCL-PVA NPs and LD-PCL-PVA NC were found to be 103.5 and 143.4 nm, with PDI of 0.351 and 0.387, respectively. This suggests that the developed nanocomposites (NCs) have a narrow particle size distribution and a homogeneous population. The Z-average size of the LD-PCL-PVA NC was slightly larger compared to the PCL-PVA, likely due to the conjugation of LD with the PCL polymer. The physical stability of the colloidal dispersion of the synthesized NC was analyzed through zeta potential as shown in Figure 1B. The zeta potential values of PCL-PVA NPs and LD-PCL-PVA NC

https://doi.org/10.1021/acsomega.5c00691
ACS Omega 2025, 10, 19682−19696

Scheme 2. Schematic Representation of Synthesis of LD-PCL-PVA NC PCL, Poly-ε Caprolactone; LD, L-DOAP; PVA, poly(vinyl alcohol); EDC, 1-ethyl-3-(3-dimethylaminopropyl)carbodiimide; NHS, N-Hydroxysuccinimide

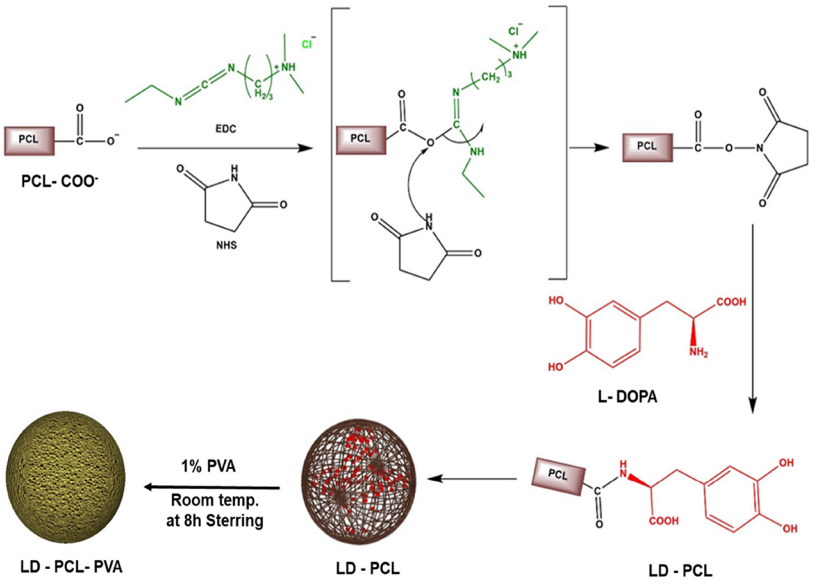

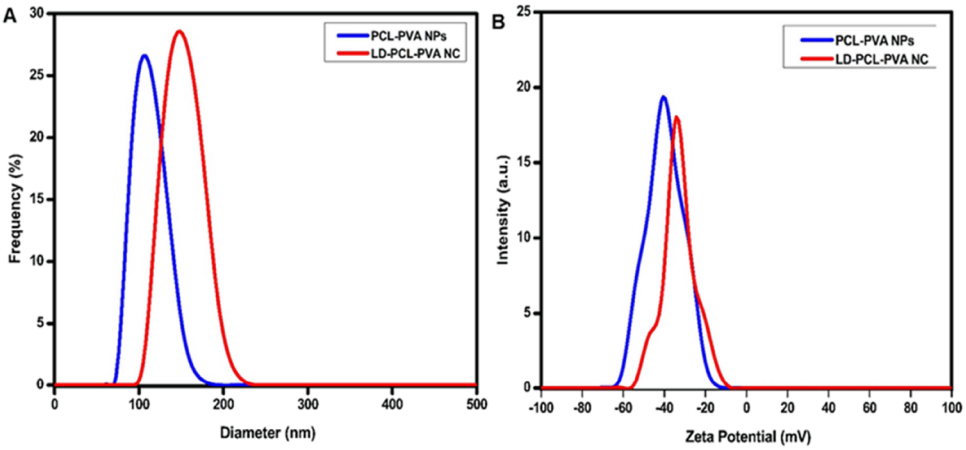

Figure 1. (A) Z average size (zeta size) of PCL-PVA NPs and LD-PCL-PVA NC. (B) Zeta potential of PCL-PVA NPs and LD-PCL-PVA NC.

were found to be −40.1 and −34.0 mV, respectively. The data indicate that the synthesized NC has sufficient repulsive force to attain better physical colloidal stability in an aqueous solution. The increased zeta potential of the LD-PCL-PVA NC compared to the PCL-PVA NPs can be attributed to the interaction of catechol groups, along with the hydroxyl and amine groups of LD, with the polymer surface. This interaction alters the surface charge by neutralizing the negative charge on the NC surface, resulting in a decrease in the overall surface charge, which can lead to the increased zeta potential of the LD-PCL-PVA NC.[40,41]

The functional groups of PCL, PCL-COO^-, PVA, LD, physical mixture (PM), and LD-PCL-PVA NC were evaluated using Fourier-transform infrared spectroscopy (Figure 2). There are possible interactions between the drug and polymer during the nanocomposite synthesis. The PCL is shown in that the characteristic band at 1723 cm^{-1} is attributed to carbonyl stretching and the bands at 1366 and 1174 cm^{-1} are, respectively, attributed to asymmetric C−O−C and symmetric C−O−C stretching. The bands appearing at 2950 and 2866 cm^{-1} correspond to asymmetric and symmetric CH_2 stretching, respectively. The FTIR spectra of PCL-COO^- reveal that characteristic bands at 1734 and 3442 cm^{-1} are respectively attributed to C═O and OH stretching, which suggests modification of PCL to PCL-COO^-[21]. In the case of PVA, the spectra exhibited the characteristic bands of PVA at 3333, 2928,1723, 1258, and 1067 cm^{-1}. These bands corresponding to the OH stretching vibration of the hydroxyl group, CH_2 asymmetric stretching, C═O carbonyl stretching, and 1258 cm^{-1} are associated with the stretching of nitrogen of C−H bonds.[42] The spectra of pure LD showed the characteristic bands at 1651 cm^{-1} corresponding to N−H bending of nitrogen of primary amine and 3202−3417 cm^{-1} corresponding to OH stretching.[43] The specific absorption bands of LD that are N−H bending (1651 cm^{-1}), along with the characteristic band of PCL-COO^- at 1734 cm^{-1}, were observed in both the physical mixture[44] and in the encapsulated nanocarrier. The spectra of the physical mixture revealed that no chemical interaction occurred between the drug and PLC. The specific groups of both the drug and PCL were observed in the spectrum of LD-PCL-PVA NC, which indicated the presence of LD in the nanocomposite.

https://doi.org/10.1021/acsomega.5c00691
ACS Omega 2025, 10, 19682−19696

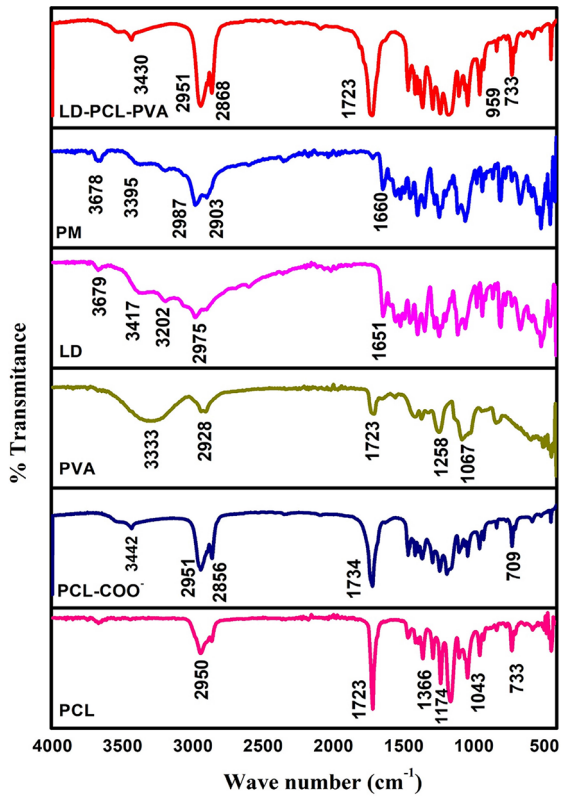

Figure 2. FTIR spectra of PCL, PCL-COO$^-$, PVA, LD, physical mixture (PM), and LD-PCL-PVA.

The external surface morphology was analyzed through FE-SEM studies. Figure 3A^1−B^1 illustrates the FE-SEM images of

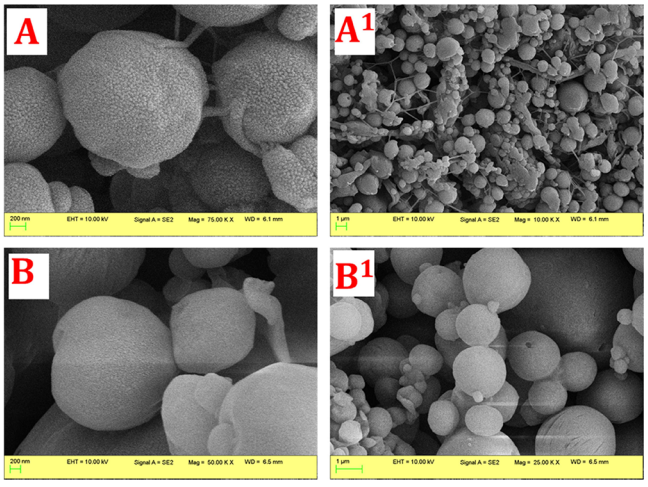

Figure 3. (A,A1) FE-SEM image of PCL-PVA NPs, (B,B1) FE-SEM image of LD-PCL-PVA NC.

PCL-PVA NPs and LD-PCL-PVA NC. The FE-SEM images of both PCL-PVA NPs and LD-PCL-PVA NC exhibited spherical structures. The PCL-PVA NP (Figure 3A,A^1) polymer surface was found to be rough in nature, and upon drug encapsulation, it turned out to be smooth. This modification of the surface morphology of LD-PCL-PVA NC (Figure 3B,B^1) confirms the LD encapsulation. The smooth surface morphology of LD-PCL-PVA NC can be attributed to the even distribution of LD within the polymer matrix.[45] The formation of a protective layer around the LD-PCL nanoparticles by PVA. This layer helps prevent particle aggregation and coalescence, leading to a smooth surface.[46]

The internal microstructure of the PCL-PVA NPs and LD-PCL-PVA NC was examined by TEM and HR-TEM analyses; the findings are shown in Figure 4A−F. The TEM images of PCL-PVA NPs (Figure 4A,A^I) exhibited a spherical shape with particle size appearing to be in the range of ∼6−22 nm, whereas the LD-PCL-PVA NC (Figure 4D,D^I) displayed slightly irregular morphology accompanied by increased particle size ranging from ∼5 to 35 nm. To estimate the average particle size, we employed *ImageJ* software by considering 55 NPs and NCs. Figure 4B,E shows the histograms of PCL-PVA NPs and LD-PCL-PVA NC. As can be seen from the histogram, the average particle size is estimated to be 12.139 and 16.03 nm for PCL-PVA NPs and LD-PCL-PVA NC, respectively. Furthermore, the HR-TEM images of PCL-PVA NPs and LD-PCL/PCL NC are shown in Figure 4C,F. The estimated *d*-spacing value is 0.371 and 0.187 nm for PCL-PVA NPs and LD-PCL/PCL NC, respectively. The decrease in *d*-spacing value due to the slight increase in the particle size of LD-PCL-PVA NC confirms the successful encapsulation of LD into PCL.[47]

Drug Encapsulation and In Vitro Release. The LD encapsulated in NC was quantified using the internal standard method using the LD standard calibration curve (r^2 = 0.999; Figure S1), and the encapsulation efficiency is 74.19 ± 2.89%. The maximum amount of LD encapsulation was obtained by using cross-linkers of EDC and the NHS, which helps to enhance drug binding bioconjugation efficiency.[48] The release of LD from the LD-PCL-PVA NC was studied for 120 h in phosphate buffer saline (pH 7.4) at 37 °C, as shown in Figure 5. The release profile indicates that 94.71% of LD was released from LD-PCL-PVA NC into PBS within a period of 120 h. A sustained LD release behavior from LD-PCL-PVA NC can be observed after 8 h. In the in vitro drug release study, the sustained LD release lasted for 120 h due to the chemical binding between the LD and the PCL-PVA polymer matrix in the developed LD-PCL-PVA NC.

In Vitro Cell Viability Assay. The 3-(4,5-dimethylthiazol-2-yl)-2,5-diphenyltetrazolium bromide (MTT) reduction test was performed to assess the cytotoxicity of developed PCL-PVA NPs and LD-PCL-PVA NC on SH-SY5Y. As illustrated in Figure 6, neither PCL-PVA NPs nor LD-PCL-PVA NC had a significant impact on cell death until 48 h, at concentrations of 100 to 400 μg/mL, demonstrating their in vitro biocompatibility. The use of doxorubicin as a positive control significantly increases cell death compared to untreated, PCL-PVA NPs and LD-PCL-PVA NC-treated cells.

Pharmacokinetic Study. LD is the most common and important prodrug for the treatment of PD, which easily crosses the blood−brain barrier and is converted into dopamine in the brain. However, it lacks pharmacokinetic properties such as half-life and bioavailability.[49,50] Therefore, the treatment efficacy is less. Hence, improving the pharmacokinetic profile of LD in the bloodstream is an important characteristic feature of its therapeutic effectiveness. In this context, improving the bioavailability of LD in the bloodstream is necessary.

After, a single dose of 23 mg/kg LD or an equal amount of LD-PCL-PVA NC was administered by intraperitoneal (IP), and LD levels in plasma were measured using LC-MS/MS as shown in Figure 7A−C. The LD level in plasma increased

https://doi.org/10.1021/acsomega.5c00691
ACS Omega 2025, 10, 19682−19696

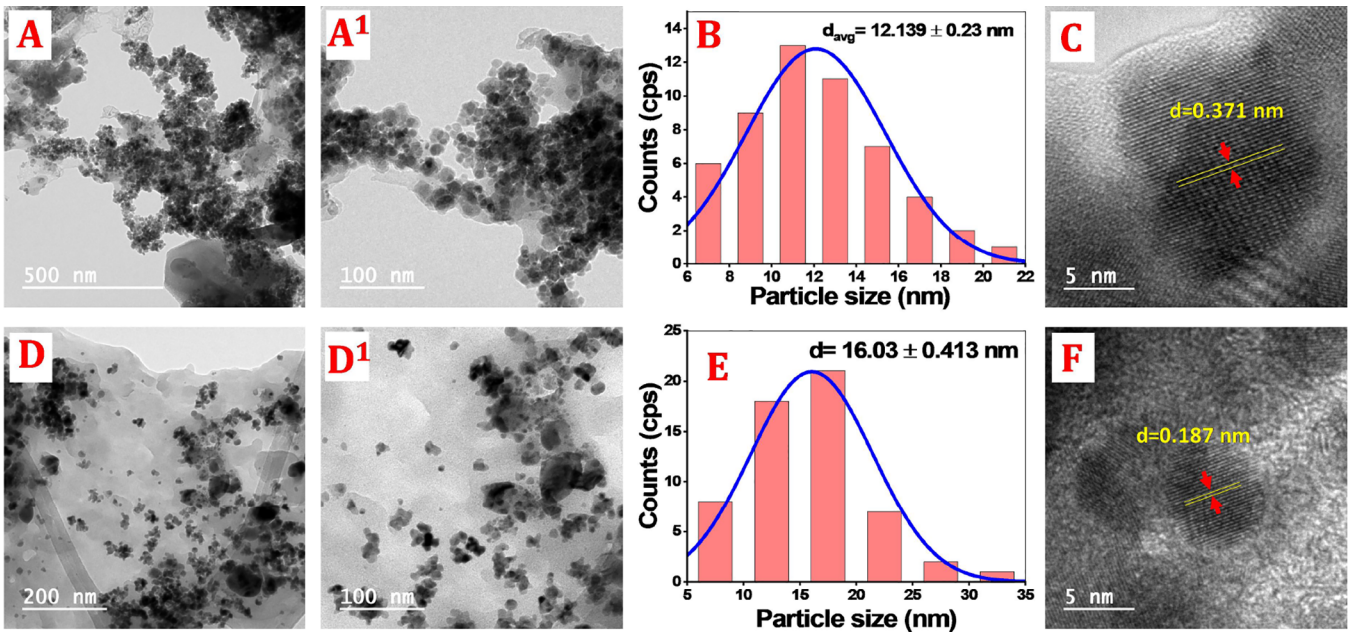

Figure 4. (A,A[1]) TEM images of PCL-PVA NPs. (B) Particle size distribution histogram. (C) HR-TEM image of PCL-PVA NPs, (D,D[1]) LD-PCL-PVA NC. (E) Particle size distribution histogram. (F) HR-TEM image of LD-PCL-PVA NC.

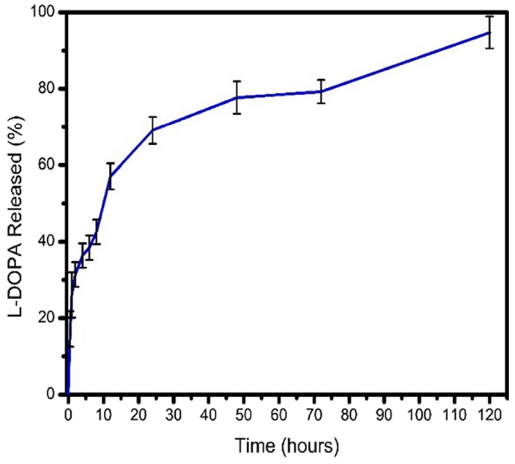

Figure 5. In vitro LD release from LD-PCL-PVA NC at time points from 0 to 120 h in phosphate buffer saline (pH 7.4).

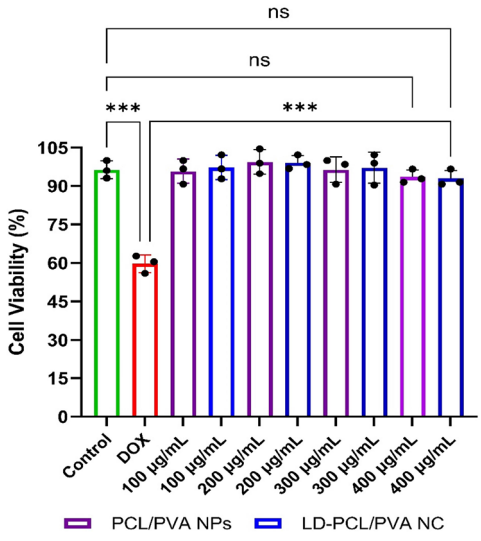

Figure 6. Effect of PCL-PVA NPs and LD-PCL-PVA NC (100−400 μg) on SH-SY5Y cells, MTT reduction assay to measure the changes in mitochondrial activity for 48 h. Data are expressed in the mean ± SEM of three individual experiments (n = 3). Significant differences compared to control indicated by ***p < 0.0001 ordinary one-way ANOVA (Tukey's post hoc test).

strictly within 30 min, but the increased level did not last long thereafter. The LD peak level declined rapidly within 1 h, with only trace amounts of LD detectable in plasma up to 3 h (Figure 7A). The plasma LD level was lower at 30 min in LD-PCL-PVA NC-administered mice compared to the standard LD administration. However, it significantly increased at 1h and was subsequently maintained up to 8 h, compared to the standard LD administration (Figure 7A). The area under the curve (AUC) is a crucial parameter in the pharmacokinetic profile. WinNonlin software 8.2 was used to calculate the AUC as shown in Figure 7B. The AUC of the LD significantly increased in LD-PCL-PVA NC-treated mice plasma compared to the AUC of the LD (P < 0.05) in standard LD-treated mice plasma. Additionally, as shown in Figure 7C, LD levels in the brain were significantly increased in LD-PCL-PVA NC-administered mice compared to standard LD-administered mice (P < 0.001).

The LC-MS/MS analysis of LD in plasma suggests that it increased within 30 min and further did not last long thereafter, which corroborates the earlier investigations.[12] The hydrophilic compound of the LD was rapidly degraded by enzymes within the systemic circulation and it undergoes decarboxylation in the gastrointestinal tract during hepatic metabolism.[9] Due to this reason, it exhibits a very short half-life under physiological conditions, resulting in the inability to reach a sufficient amount of LD in the brain, which leads to the failure to prevent the symptoms of PD for a long time.[51] The LD level in LD-PCL-PVA NC-administered mice plasma was maintained for up to 8 h. LD strongly binds with an inside core of the PCL matrix and takes time to release the LD inside the core of PCL-PVA NPs into plasma; in this situation, the brain

https://doi.org/10.1021/acsomega.5c00691
ACS Omega 2025, 10, 19682−19696

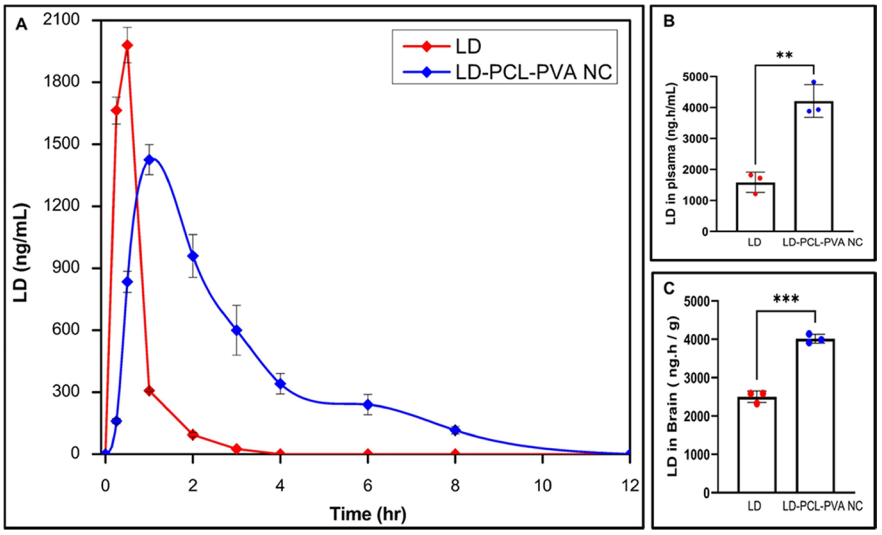

Figure 7. Pharmacokinetic profile of a single dose IP injection of LD and LD-PCL-PVA NC. (A). The amount of LD in mice' plasma after a single dose ip injection of LD and LD-PCL-PVA NC. (B) Area under the curve (AUC) value of LD in the mice plasma. (C) Area under the curve (AUC) value of LD in the mouse brain. Data are expressed as mean ± SEM (**p > 0.001, ***p < 0.0001).

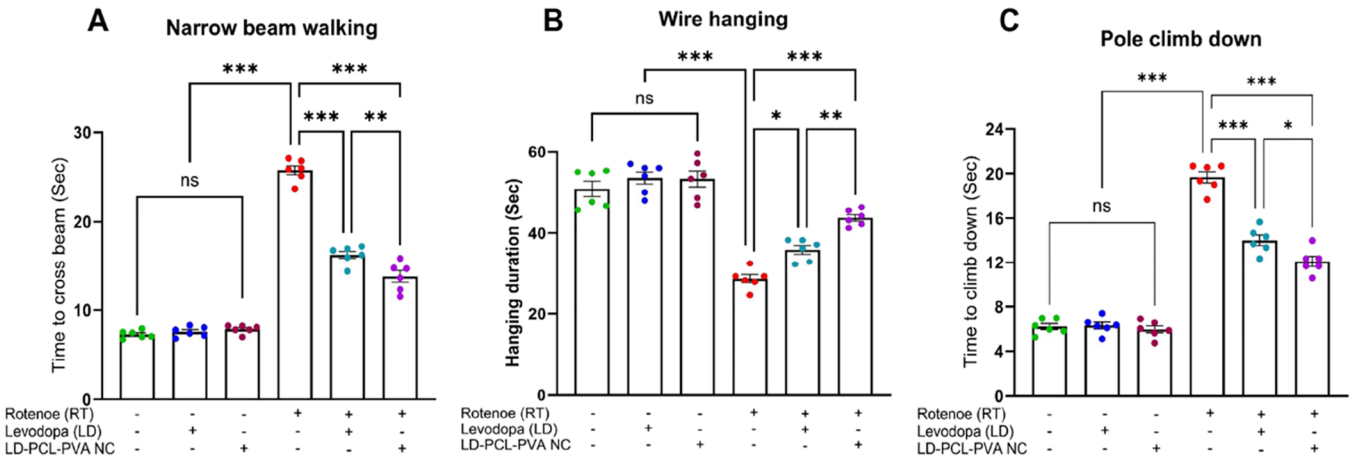

Figure 8. Effect of LD-PCL-PVA NC, LD, ROT and cotreatment of ROT with LD-PCL-PVA NC and LD for 21 days, on (A) Narrow beam walking test, (B) Wire hanging test and (C) Pole test of mice. Data are expressed in the mean ± SEM (n = 6), significant differences compared to control indicated by *p < 0.05, **p > 0.001 and ***p < 0.0001; Ordinary one-way ANOVA (Tukey's post hoc test).

receives the maximum amount and long-term presence of LD that escapes from rapid metabolism in plasma. Thus, LD-PCL-PVA NC has a significant impact on improving the bioavailability in plasma.

Therapeutic Effect of LD-PCL-PVA NC on ROT-Induced PD Mice. ROT has been widely used as an experimental model to induce PD. It was easily able to cross the BBB and inhibit the classic mitochondrial complex I of the electron transport chain, leading to the progressive loss of DPN.[52] ROT also causes the aggregation of α-synuclein protein and the activation of glial cells, which further causes DPN death.[53] In the current study, 2.5 mg/kg of ROT was used to induce PD symptoms in mice for 21 days. The mortality did not occur among the control, induced, and treatment groups; the dose of rotenone used in the study was sublethal and within a range that induces motor dysfunction without causing fatality. The ROT-treated group mice did not gain weight (Figure S5); these results corroborate with the earlier investigation.[54,55] The LD and LD-PCL-PVA NC-treated mice did not lose body weight, as shown in Figure S5.

Behavior Study. The narrow beam walking, pole climbing, and wire hanging tests are well-established tests to assess walking, balance, vestibular integrity, muscular coordination, impairment of limb movement, and neuromuscular strength in PD-induced animals.[56] The performed evaluation shows that the ROT-induced PD imposes defective motor symptoms, as shown in Figure 7A–C. ROT-induced PD mice showed a significant increase in the narrow beam crossing time (Figure 8A) and pole climb-down time (Figure 8C). Additionally, a significant decrease in the wire hanging time (Figure 8B) compared to the control group (P > 0.0001). The behavioral tests performed on ROT-induced mice treated with LD and LD-PCL-PVA NC showed significant improvement compared to ROT-induced PD mice. But, the LD-PCL-PVA NC-treated ROT-induced PD mice significantly improved the narrow beam crossing time (Figure 8A), pole climb downtime (Figure 8C), and wire hanging time (Figure 8B) compared to the LD-treated ROT-induced PD mice (p > 0.001 and P > 0.05, respectively).

https://doi.org/10.1021/acsomega.5c00691
ACS Omega 2025, 10, 19682−19696

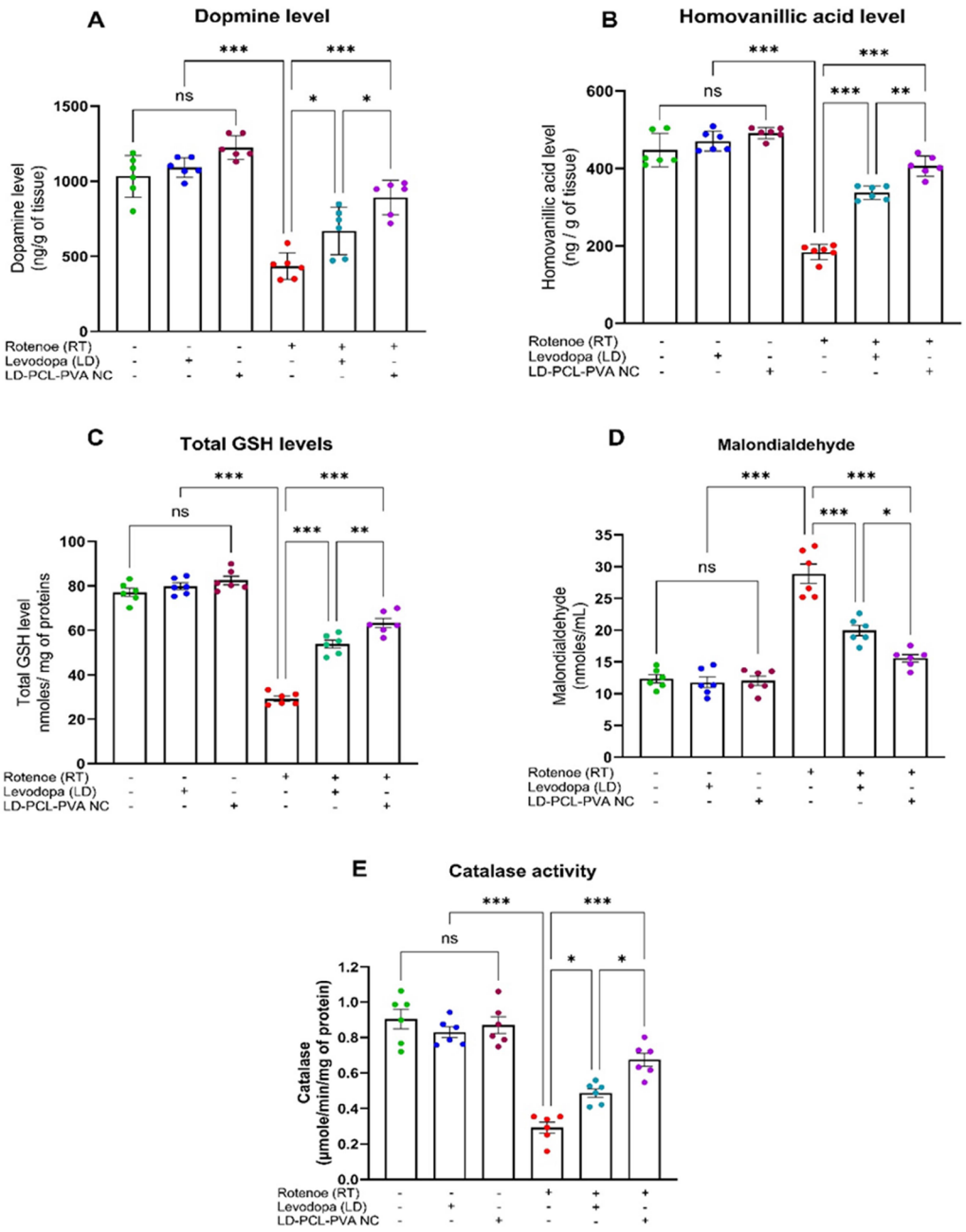

Figure 9. Effect of LD-PCL-PVA NC, LD, and ROT and cotreatment of ROT with LD-PCL-PVA NC and LD for 21 days, on (A) Dopamine level, (B) Homovanillic acid level, (C) Total GSH level, (D) malonaldehyde, and (E) catalase activity of mice brain. Data are expressed in the mean ± SEM ($n = 6$), with significant differences compared to control indicated by *$p < 0.05$, **$p > 0.001$, and ***$p < 0.0001$; Ordinary one-way ANOVA (Tukey's post hoc test).

ROT has been proven to have an impact on motor symptoms in various previous studies, including mice.[57,58] In the present study, ROT administration resulted in a decline in motor behavior in mice, evident by the increased pole climb-down time, longer beam crossing time, and reduced grip strength. This suggests an induction similar to that observed in idiopathic disease.[59] Based on the behavioral assessment, it can be concluded that LD-PCL-PVA NC may be more effective in improving impaired movement in the rotenone-induced PD mice model compared to LD-treated PD mice. The LD only improved the latency time of PD-induced mice, but the enhancement of LD bioavailability in plasma and brain by LD-PCL-PVA NC significantly restored the motor symptoms in ROT-induced PD mice. A previous study indicated that LD treatment in PD mice only improved the latency time in motor tests.[12,46] However, our finding demonstrates a significant improvement in motor deficits upon treatment with LD-PCL-PVA NC, which is due to the enhancement of the bioavailability of LD in the plasma and DA in the brain.

DA and HVA Levels. The DA and HVA levels of mice brains were measured using an HPLC-ECD as shown in Figure 9A,B. The ROT-induced mice showed a significant loss of 2.2-fold in the DA level (F (5,30) = 40.44; $P < 0.0001$; Figure 9A) compared to the control. The ROT plus LD and LD-PCL-PVA NC showed a significant increase of 1.47 and 1.95 folds, respectively, in the DA level compared to the ROT-induced

https://doi.org/10.1021/acsomega.5c00691
ACS Omega 2025, 10, 19682−19696

PD mice (F (5,30) = 40.44; P < 0.05 and P < 0.0001, respectively; Figure 9A). However, ROT plus LD-PCL-PVA NC-treated mice showed a significant increase of 1.3-fold in DA level compared to ROT plus LD-treated mice (F (5,30) = 40.44; P < 0.05; Figure 9A).

Compared to the control mice, ROT-induced mice showed a significant decrease of 2.42-fold in the HVA level (F (5,30) = 35.86; P > 0.0001; Figure 9B). The ROT-induced mice treated with LD and LD-PCL-PVA NC showed a significant increase of 1.88 and 2.18 folds, respectively, in the HVA level compared to ROT-induced PD mice (F (5,30) = 35.86; P > 0.0001; Figure 9B). The ROT plus LD-PCL-PVA NC-treated mice showed a significant increase of 1.15fold in the HVA level compared to the ROT plus LD-treated mice (F (5,30) = 35.86; P > 0.001; Figure 9B).

A monoamine catecholamine, DA, is an important neurotransmitter that plays an important role in motor and nonmotor functions.[60] HVA is a primary metabolite of DA and plays a crucial role in metabolic stress and understanding brain functions. DOPAC and HVA are excellent controls for monitoring changes in metabolism in the CNS dopamine.[61] Several studies have indicated reduced DA and HVA levels by ROT in mice.[62] In the current study, the decreased level of DA and HVA by ROT in mice also showed that LD-PCL-PVA NC significantly restores the DA and HVA levels in ROT-induced mice compared to LD alone treatment.

Biochemical Stress Markers. The total GSH, MDA, and catalase activities are considered biochemical markers for stress. Therefore, the effect of LD-PCL-PVA NC on ROT-induced PD mice was analyzed (Figure 9C–E). In ROT-induced PD mice, the total GSH level was significantly decreased by 2.74 fold compared to the untreated mice (F (5,12) = 68.24; P < 0.0001; Figure 9C). Mice treated with ROT along with LD and LD-PCL-PVA NC showed a significant increase of 1.87 and 2.19 folds, respectively, in the total GSH level, compared to the ROT-induced PD mice (F (5,12) = 68.24; P < 0.0001; Figure 9C). ROT plus LD-PCL-PVA NC showed a significant increase of 1.17 fold in the total GSH level compared to ROT plus LD treated ROT-induced PD mice (F (5,12) = 68.24; P < 0.001, Figure 9C). Control groups of LD and LD-PCL-PVA NC did not show any significant changes in GSH activity compared with untreated mice.

The ROT-induced PD mice showed a significant increase of 2.20-fold in MDA activity, compared to the control mice (F (5,12) = 28.24; P > 0.0001; Figure 9D). The mice treated with ROT plus LD and LD-PCL-PVA NC showed a significant decrease of 1.33 and 1.59 fold, respectively, in MDA activity, compared to ROT-induced PD mice (F (5,12) = 28.24; P > 0.0001; Figure 9D). Compared to ROT plus LD, the LD-PCL-PVA NC showed a significant increase of 1.18-fold in MDA activity (F (5,12) = 28.24; P > 0.05; Figure 9D). Control groups of LD and LD-PCL-PVA NC did not show a significant change in MDA activity compared with control mice.

Compared to the control group, ROT-induced PD mice showed a significant increase of 2.58 folds in Catalase activity (F (5,12) = 15.41; P < 0.0001; Figure 9E). Treatment of mice with ROT plus LD and LD-PCL-PVA NC showed a significant increase of 1.43 and 1.97 fold respectively in catalase activity, compared to ROT-induced PD mice (F (5,12) = 15.41; P < 0.05 and P < 0.0001 respectively; Figure 9E), and ROT plus LD-PCL-PVA NC showed a significant increase of 0.78 fold in catalase activity compared to ROT plus LD treated PD mice (F (5,12) = 15.41; P < 0.05; Figure 9E). The control groups LD and LD-PCL-PVA NC did not exhibit any notable changes in catalase activity compared with untreated mice.

Previous studies have suggested that the dopaminergic neurons in PD are constantly exposed to oxidative stress.[63] The main powerhouse of ROS production is the mitochondria and its dysfunction leads to increased production of ROS, which causes degeneration of dopaminergic neurons by causing oxidative stress.[64,65] In the current study, we found that ROT is responsible for oxidative damage, which inhibits the mechanistic function of antioxidant enzymes, as shown in previously reported studies.[66,67] It is observed that LD-PCL-PVA NC significantly increases the antioxidant enzymes, GSH and catalase activity while significantly decreasing the MDA level. Recent studies have reported that LD restores ROT-damaged oxidative stress, such as GSH, MDA, and catalase activity.[66,68] The present study compared LD, and LD-PCL-PVA NC significantly restores the GSH, MDA and catalase activity, which may lead to sustained and long-term release of LD in the brain.

Histopathology Studies. In nanomedicine, biocompatibility is crucial for the successful clinical translation of nanotherapeutics. In this context, key organs such as the brain, lungs, heart, liver, and kidneys were collected to evaluate pathological changes following treatment with LD and LD-PCL-PVA NC. The results obtained from the H&E staining (Figure S6) showed that the major organs, including the brain, liver, heart, and kidneys, remained in a healthy condition, with no significant signs of inflammation or other pathological changes observed. Based on the H& E result, we selected 7.5 mg/kg of LD or equivalent LD-PCL-PVA NC 21-day treated mice that did not cause toxicity.

CONCLUSIONS

In the current study, the synthesized LD-PCL-PVA NC exhibited improvement in the bioavailability in plasma and brain; in addition, it mitigated the behavioral and molecular defects observed in the ROT-induced PD mice model. PCL-PVANPs and LD-PCL-PVA NC did not show significant toxicity on the SH-SY5Y cell line, and long-term treatment with LD-PCL-PVA NC did not cause noticeable toxicity in mice. The single dose intraperitoneal injection of LD-PCL-PVA NC significantly improved the bioavailability in mice' plasma and brains compared to the standard LD. Interestingly, treatment with LD-PCL-PVA NC significantly improved the motor symptoms, neurotransmitter, and biochemical stress markers in the ROT-induced PD mice model. Based on the obtained results, the study states that the LD-PCL-PVA NC formulation may provide a novel therapeutic approach for improving the bioavailability, biodistribution, motor symptoms, and neurotransmitters for effective treatment of PD. The study suggested that LD-PCL-PVA NC can be used for effective and promising treatment of PD.

MATERIALS AND METHODOLOGY

Materials. Poly-ε-Caprolactone (PCL; CAS No.24980-41-4), Poly (vinyl alcohol) (PVA; CAS No. 9002-89-5), dichloromethane (DCM; CAS No. 75-09-2), dl-10-camphor sulfonic acid (C10H16O4S; CAS No. 35963-20-3), isoflurane (CAS No. 26675-46-7), acetonitrile (CAS No. 75-05-8), formic acid (CAS No. 64-18-6), Rotenone (CAS No. 83-79-4), Dimethyl sulfoxide (DMSO; CAS No. 87893-62-7), Homo-

https://doi.org/10.1021/acsomega.5c00691
ACS Omega 2025, 10, 19682−19696

vanillic acid (HVA; CAS No. 306-08-1), Perchloric acid (CAS No. 7601-90-3), Triethylamine (TEA; CAS no. 121-44-8), Formalin solution (Product No. HT501640) were purchased from Sigma-Aldrich, USA. Levodopa (LD; CAS No. 59-97-7), Dopamine hydrochloride (CAS No. 62-37-7), 1-Ethyl-3-(3-dimethylaminopropyl) carbodiimide (EDC; 99−102%; CAS No. 25962-53-8), N-Hydroxy succinimide (NHS; 97−103%; CAS No. 6066-82-6), Sodium hydroxide (NaOH; CAS No. 1310-73-2), Ammonium acetate, HPLC grade (CAS No.: 631-61-8), Ethylenediaminetetraacetic acid (EDTA; CAS No. 6281-92-6), Citric acid (CAS No. 5949-29-1), 3-(4,5-dimethylthiazol-2-yl)-2,5-diphenyltetrazolium bromide (MTT); Antibiotic Antimitotic Solution 100X Liquid (A002A-20 ML), Dulbecco's Modified Eagle Medium (DMEME; AL0078−500 ML), and Fetal Bovine Serum (FBS; RM1112-500ML) were purchased from HIMEDIA Laboratories Private Limited in India. Methanol (CAS No. 67-56-1) was purchased from the Statutory Liquidity Ratio (SLR) in India. All chemicals were of reagent grade, used as received, and stored according to manufacturer guidelines. All of the aqueous solutions were prepared using Millipore and double-distilled water.

Synthesis of LD-PCL-PVA NC. In the first step, the end group modification of PCL was carried out by immersing 1 g of PCL pellet in 1 N sodium hydroxide (100 mL) for 4h in constant shaking at 37 °C. The obtained PCL-COO^- was washed with double-distilled water and stored in an airtight bottle until further use.[21] The preparation procedure for PCL-COO^- is shown in Scheme 1.

In the second step, the LD-PCL-PVA NPs were synthesized by the double emulsion solvent evaporation method based on the method described by Pahuja et al.,[18] with some modifications. Briefly, 100 mg of PCL-COO^- was dissolved in 10 mL of DCM, followed by the addition of 40 mg of EDC and 60 mg of NHS. The mixture was refluxed at 30 °C for 2 h. Furthermore, 2 mL of LD (3.3 mg/mL) was added dropwise to the above solution with an 800-rpm starting speed. The mixture was further sonicated for 5 min to obtain the primary water/oil emulsion, and the obtained emulsion was added to 40 mL of 1% PVA with 1500 rpm stirring speed and sonicated for 5 min to obtain the water/oil/water emulsion. The following emulsion was continued to stir for 8 h and centrifuged at 8000 rpm for 30 min at 4 °C and washed to remove the unbound drug. Finally, the obtained LD-PCL-PVA NC were freeze-dried and stored at 4 °C (Scheme 2).

Characterization of LD-PCL-PVA NC. The FTIR studies of LD, PCL, PVA, PCL-PVA NPs and LD-PCL-PVA NC were carried out using a Nicolet impact-410 FTIR spectrometer, USA (University Science Instrumentation Facility, phase-II, Karnatak University, Dharwad, India). The particle Z-average size, zeta potential, and PDI of PCL-PVA NPs, LD-PCL-PVA NC were analyzed by dynamic light scattering using a HORIBA scientific, SZ-100, Ver2.20 (University science instrumentation facility phase-II, Karnatak University, Dharwad, India). The synthesized NCs were characterized for their shape, surface morphology, and particles size distributions by using FE-SEM (Carl Zeiss, Germany. Model. SUPRA 55; Chloros Energy Material Characterization Centre Tumkuru, India) and transmission electron microscope (JEOL JEM 2100 PLUS) were used to detect the internal microstructure of synthesized PCL-PVA NPs and LD-PCL-PVA NC.

Drug Encapsulation Efficiency. The drug encapsulation efficiency was determined by using an HPLC-UV detector. In LD-PCL-PVA NC, the measurement was done indirectly by estimating the unencapsulated LD in the supernatant after separating the NC at 10,000 rpm for 35 min. The obtained supernatant was filtered using a 0.2 μm syringe filter, and 20 μL of the sample was injected into an HPLC-UV detector (PerkinElmer). The separation was done on a C-18 column (4.6 × 250 mm length and 5 μm diameter; Shimadzu Shim-pack) using the mobile phase 950 mL of ammonium acetate buffer (pH 4) and 50 mL of methanol was used in isocratic mode. The flow rate of 1 mL/min for 10 min and RT is 4.9 min. The peak of the LD was identified at 280 nm and quantified using an LD standard calibration curve (r^2 = 0.998; Figure S1). The encapsulation efficiency (EE) was calculated by using the following formula.[15,69]

$$\text{EE (\%)} = \frac{\text{Total amount of LD} - \text{unencapsulated LD in supernatant}}{\text{Total amonut of LD}}$$

In Vitro Drug Releasing Assay. In vitro release kinetics of LD release from LD-PCL-PVA NC were determined by using the dialysis method as described by Ngwuluka et al.,[70] and Nie et al.[46] In brief, 10 mg of LD-PCL-PVA NC were dispersed in 30 mL of PBS (pH 7.4) and transferred into a dialysis membrane (Spectra/Por; Molecular cutoff, 12−14 kDa). The membrane was allowed to dialyze against 30 mL of PBS with constant stirring at 100 rpm in a shaker incubator at 37 °C (lab companion; SIF6000R). At different time points, 1 mL of aliquots was withdrawn, and the same amount of fresh buffer was replaced. The absorbance of the sample was measured at 280 nm (UV−visible spectrophotometer). The amount of released LD was calculated using a LD calibration curve of LD in PBS (r^2 = 0.998; Figure S2).

In Vitro Cell viability Assay on SH-SY5Y. The human neuroblastoma cell line SH-SY5Y was purchased from NCCS Pune, Maharashtra, India. The SH-SY5Y cell line was cultured in DMEM medium containing 10% fetal bovine serum with Antibiotic Antimycotic Solution at a constant temperature of 37 °C with 5% CO_2. The cell culture medium was changed every two days.

Cell viability assay was conducted based on the method described by Luo et al.,[71] to determine the effect of LD-PCL-PVA NC and PCL-PVA NPs on mitochondrial integrity. The SH-SY5Y cells were seeded with 5 × 10^4 cells per well in a 96-well plate and incubated overnight. Cells were treated with different concentrations of PCL, PVA, LD-PCL-PVA NC and PCL-PVA NPs (100, 200, 300, and 400 μg/mL) at 48 h. After 48 h treatment, 10 μL of MTT (5 mg/mL) was added to each well, and the mixture was incubated at 37 °C for 4 h under 5% of CO_2. The formazan crystals were dissolved in 100 μL of DMSO. The absorbance of formazan crystals was measured at 595 nm using a multiwall microplate reader (BioTek Epoch 2 Microplate Reader, Agilent) and the viability of cells was calculated as a percent of the untreated control.

Animals. The adult male BALB/c mice of eight to 10 weeks old (28−30 g) were procured from Chromed Biosciences Pvt. Ltd., Tumkur, Karnataka, India. Each cage contained three animals, which were kept under a 12-h light/dark cycle at a temperature of 25 ± 2 °C, with free access to food and water. The animals were acclimatized for at least 5 days before the study. The handling and experimentation were approved by the Institutional Animal Ethics Committee (IAEC), Chromed Biosciences Pvt. Ltd., India (Approved number CBPL-IAEC-077/04/2024).

https://doi.org/10.1021/acsomega.5c00691
ACS Omega 2025, 10, 19682−19696

Pharmacokinetic Analysis. The pharmacokinetic study was conducted based on the method described by Vong et al.[12] 23 mg/kg of LD or LD equivalent LD-PCL-PVA NC was injected intraperitoneally into BALB/c mice (body weight 28 ± 2 g). Furthermore, at the predominant time interval, mice were deeply anesthetized using isoflurane inhalation, and blood was collected from the retro-orbital sinus. Simultaneously, the animal was sacrificed, and the brain tissues were collected for further analysis. The plasma was separated from blood by centrifugation (REMI cooling centrifuge C-24 BL) at 10,000 rpm for 10 min. Collected plasma and brain tissues were stored at −80 °C until further analysis.

Plasma and Brain Tissue Preparation for LC-MS/MS. The tissue was homogenized with 10 mM phosphate buffered saline (pH 7.4; 1:5 w/v); 100 μL of tissue homogenate obtained was precipitated with 225 μL of acetonitrile with an internal standard (500 ng of Tolbutamide in 1 mL of acetonitrile) for 10 min, and the mixture was centrifuged at 10,000 rpm. The obtained supernatant was diluted with Mili-Q water (1:1) and used for analysis.

LC-MS/MS System. The amount of LD in plasma and tissue samples was quantified using an LC-MS/MS (XEVO-TQ-S-CRONOS) system with an Inertsil ODS-3 column (Column size 4.6 × 100 nm). The mobile phase consists of 0.1% formic acid in water and 0.1% formic acid in acetonitrile; it was pumped at a flow rate of 0.8 mL/min. Tolbutamide was used as an internal standard.

Treatment Procedure. 50 mg of ROT was dissolved in 1 mL of DMSO, from an aliquot 0.2 mL of ROT was diluted with 19.8 mL of saline containing DMSO (0.1%), and the ROT final concentration of 1 μg/2 μL was used for the study. Each time, freshly prepared ROT was used for all the experiments.[72]

After five days of acclimatization, 108 (N = 18) adult male mice were divided into six groups randomly; each group contained 18 animals; (1). Control group: Normal saline (n_1 = 18); (2). LD control group: Animals received a single intraperitoneal (ip) injection of LD (7.5 mg/kg body weight)[73,74] daily until 21 days (n_2 = 18); (3). LD-PCL-PVA NC control group: Animals received a single ip injection of LD-PCL-PVA NC (equivalent to 7.5 mg/kg body weight LD) daily until 21 days (n_3 = 18); (4). ROT positive control group: Animals received a single ip injection of ROT (2.5 mg/kg body weight RT)[74−77] daily until 21 days (n_4 = 18); (5). ROT+LD treatment group: Animals received a single ip injection of both ROT and LD simultaneously (2.5 mg/kg body weight ROT; 7.5 mg/kg body weight LD) daily until 21 days (n_5 = 18); (6). ROT+LD-PCL-PVA NC group: Animals received a single ip injection of both ROT and LD-PCL-PVA NC simultaneously (2.5 mg/kg body weight ROT; equivalent to 7.5 mg/kg body weight LD) daily until 21 days (n_6 = 18).

After acclimatization, all mice underwent training on the narrow beam, pole climb-down, and wire hanging apparatus. Following 5 days of training, the treatment was started and considered as day one. During the treatment period, the body weights of all mice were recorded daily and monitored for food intake. On the 21st day, the last IP administration, behavior assay was conducted. Furthermore, mice were euthanized by carbon dioxide asphyxiation, and the brain tissues were used for the analysis of neurotransmitters and biochemical evaluation. Similarly, the brain, lungs, heart, liver, and kidney were also used for the histopathology evaluation (Scheme 3).

Scheme 3. Scheme of Detailed Experimental Design, the Effect of LD Encapsulated Polycaprolactone Nanocomposite (LD-PCL-PVA NC), Levodopa (LD), Rotenone (ROT) and Co-treatment of ROT with LD-PCL-PVA NC and LD on Mice for 21 days

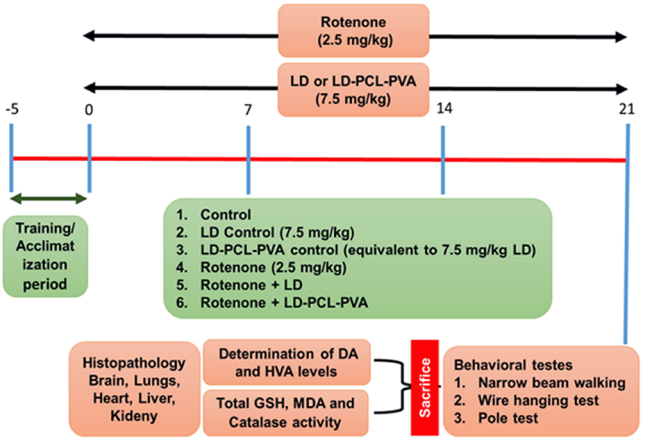

Behavioral Studies. *Narrow Beam Walking.* As previously described by Singh et al.[78] and Venkatesh Gobi et al.,[79] the narrow beam walking assay was performed. To reach an enclosed area, the mice were pretrained to cross an elevated and narrow beam. At the end of the experiment, mice were allowed to transfer the narrow 100 cm length × 1 cm width flat wooden beams, which were placed at a height of 100 cm from the ground. The duration of the journey from the starting point to the end point was recorded. Each mouse was tested in three trials, and the average time was calculated for further analyses.

Pole Test. The pole test was carried out using the method described by Wang et al.[62] Briefly, the mice were placed on a wooden pole with a diameter of 1 cm and a length of 50 cm. The time taken to climb down to the floor was recorded. Each mouse was tested three independent times, and the average time was calculated for the analysis.

Wire Hanging Test. According to the method described by Badawi et al.,[80] and El-Shamarka et al.,[81] a wire-hanging test was conducted. A 25 cm-long horizontal wire was placed at a height of 0.25 m above the working table and held the mice's forelimbs. The time it takes for mice to fall off the wire was recorded; each mouse was tested in three independent trials, and the average time was calculated for analysis.

Determination of DA and HVA Levels. The method described by Hanumanthappa et al.,[8] Pahuja et al.,[18] and Smruthi et al.,[69] was used to determine the DA and HVA in brain tissue. Briefly, Brain tissues were homogenized using 2 N perchloric acid and the homogenate was centrifuged at 1000 rpm (REMI cooling centrifuge C-24 BL) for 10 min at 4 °C and filtered through a 0.2 μm syringe (AXIVA syringe filter nylon-13 mm/0.2 μm). After, 20 μL of supernatant was injected into the HPLC system (C-18 column: Spherisorb, RP C18, 5 μm particle size, 4 × 250 mm at 30 °C; electrochemical detector: model 1645, Waters, USA). The mobile phase consists of 17.6% methanol, 82.4% water, 0.0876 mM of EDTA, 1.5 mM of TEA, 9 mM of dl-$C_{10}H_{16}O_4S$, 20 mM Na_2HPO_4, and 15 mM citric acid (pH 4.2). It was pumped at a flow rate of 1.5 mL/min. The DA and HVA concentration in the sample was analyzed by comparing it with the standard peak area (Figures S3 and S4) and expressed as ng/g of tissue.

https://doi.org/10.1021/acsomega.5c00691
ACS Omega 2025, 10, 19682−19696

Biochemical Assay. *Homogenate Preparation for Biochemical Assay.* The mouse striatum tissue was homogenized with 0.1 M phosphate buffer (pH 7.4; 1:4 w/v) and the homogenate was centrifuged at 10,000 g for 10 min at 4 °C (REMI cooling centrifuge C-24 BL). The obtained supernatant was used for the following biochemical parameters: protein estimation, reduced glutathione level (GSH), malonaldehyde level (MDA) and catalase activity.

Total Protein Estimation. The total protein concentration of tissue homogenate was estimated using BSA as the standard.[82,83]

Determination of the GSH Level. The GSH level was determined according to the method described by Mbiydzenyuy et al.,[66] using DTNB reagent. The homogenate was precipitated with an equal volume of 4% sulfosalicylic acid, and the mixture was incubated for 1 h at 4 °C. The resulting mixture was centrifuged at 10 min (2000 rpm, 4 °C). Finally, the supernatant was mixed with 10 mM DTNB (1.8 mL), and the reaction mixture was observed at 412 nm against a blank using a UV−visible spectrophotometer. The data are expressed as μmol per mg of protein.

Determination of the MDA Level. The MDA level was determined as previously described by Samokyszyn et al.,[72] and Parthasarathy et al.,[84] using thiobarbituric acid. The reaction mixture containing homogenate, 10% TCA, and 0.67% TBA in a final volume of 1.0 mL was heated at 95 °C for 10 min. It was further allowed to cool, and after cooling, the reaction mixture was centrifuged at 7000 rpm for 10 min and measured at 530 nm using a UV−visible spectrophotometer. The data was expressed as nmol MDA per mL.

Determination of Catalase Activity. Catalase activity was determined, as described by Hanumegowda et al.,[85] and Parthasarathy et al.[84] In brief, the reaction mixture consisted of 800 μL of 50 mM phosphate buffer (pH 7.0), 180 μL of hydrogen peroxide (300 mM), and 20 μL of the sample. The loss of absorbance of hydrogen peroxide was measured at 240 nm for 2 min at every 10 s interval at 25 °C using a UV−visible spectrophotometer. The catalase activity was expressed as μmol of H_2O_2 per mg of protein.

Histopathology Studies. After the animal was sacrificed, the vital organs such as the brain, heart, liver, kidney, and spleen were dissected and fixed in 10% buffered formalin. The tissue was trimmed and processed using a TP 1020 automated tissue processor (Leica, Germany). Further, paraffin-embedded (Histo-Core, Areadia H) samples were subsequently sliced into 4 μm thickness using a microtome (Leica RM2125 RTS, Germany) and stained with Haematoxylin and Eosin (H&E). Histological assessment was observed under light microscopy (OLYMPUS CX33, Japan) to evaluate the potential toxicity of the LD and LD-PCL-PVA NC.

Statistical Analysis. Graph Pad Prism 10.2.3 software was used for statistical analysis and plotting graphs; for ordinary one-way ANOVA (Tukey's post hoc test) of mean ± SEM, for $n = 6$, significant differences compared control indicated by $^*p < 0.05$, $^{**}p > 0.001$ and $^{***}p < 0.0001$; For Pharmacokinetic Study, t test values $^{**}p > 0.05$, $^{***}p < 0.001$ were considered statistically significant (mean ± SEM, for $n = 3$). WinNonlin software 8.2 was used to calculate the AUC of LD in mice' plasma and brain.

■ ASSOCIATED CONTENT

Supporting Information

The Supporting Information is available free of charge at https://pubs.acs.org/doi/10.1021/acsomega.5c00691.

Levodopa standard calibration curve (Figure S1) by HPLC-UV for calculating the DE, levodopa standard calibration curve by UV−visible spectroscopy (Figure S2) for drug releasing studies, dopamine standard curve (Figure S3) by HPLC-ECD for determination of the DA level in the mouse brain, homovanillic acid standard curve (Figure S4) by HPLC-ECD for determination of HVA levels in mice brain, animal body weight during treatment days (Figure S5), and histopathology studies (Figure S6) (PDF)

■ AUTHOR INFORMATION

Corresponding Author

Kuramkote Shivanna Devaraju − *Neuro-Chemistry Lab, Department of Biochemistry, Karnatak University, Dharwad, Karnataka 580003, India;* orcid.org/0000-0002-6199-354X; Email: ksdevaraju@kud.ac.in, devarajuks@gmail.com

Authors

Ramesha Hanumanthappa − *Neuro-Chemistry Lab, Department of Biochemistry, Karnatak University, Dharwad, Karnataka 580003, India*

Geetha B. Heggannavar − *Department of Chemistry, Karnatak University, Dharwad, Karnataka 580003, India*

Aishwarya Banakar − *Central Research Laboratory, SDM College of Medical Sciences and Hospital, Shri Dharmasthala Manjunatheswara University, Dharwad, Karnataka 580 009, India*

Divya D. Achari − *Department of Chemistry, Karnatak University, Dharwad, Karnataka 580003, India*

Vijaykumar Ramesh Karoshi − *Nutrition, Biochemistry and Toxicology Division, Defence Food Research Laboratory (DRDO−DFRL), Mysore 570011, India*

B. R. Radha Krushna − *Prof. C.N.R. Rao Centre for Advanced Materials, Tumkur University, Tumkur 572 103, India*

Asmatanzeem Bepari − *Department of Basic Health Sciences, College of Medicine, Princess Nourah bint Abdulrahman University, Riyadh 11671, Saudi Arabia;* orcid.org/0000-0001-7633-2923

Rasha Assad Assiri − *Department of Basic Medical Sciences, College of Medicine, Princess Nourah bint Abdulrahman University, Riyadh 11671, Saudi Arabia*

Hanan Nasser Altamimi − *Department of Medical Laboratory, College of Applied Medical Sciences, Prince Sattam Bin Abdul-Aziz University, Al-Kharj 11942, Saudi Arabia*

Hemalatha Nanjaiah − *Neuro-Chemistry Lab, Department of Biochemistry, Karnatak University, Dharwad, Karnataka 580003, India; Department of Microbiology and Immunology, University of Maryland School of Medicine, Baltimore, Maryland 21201, United States*

Devaraja Sannaningaiah − *Department of Studies and Research in Biochemistry and Centre for Bioscience and Innovation, Tumkur University, Tumkur 572 103, India*

Shamprasad Varija Raghu − *Division of Neuroscience, Yenepoya Research Centre (YRC), Yenepoya (Deemed to be University), Mangalore, Karnataka 575 018, India*

Vishwas Kaveeshwar − *Central Research Laboratory, SDM College of Medical Sciences and Hospital, Shri Dharmasthala Manjunatheswara University, Dharwad, Karnataka 580 009, India*

H. Nagabhushana − *Prof. C.N.R. Rao Centre for Advanced Materials, Tumkur University, Tumkur 572 103, India;* orcid.org/0000-0001-7552-3373

Complete contact information is available at: https://pubs.acs.org/10.1021/acsomega.5c00691

Author Contributions

Conceptualization − K.S.D. and R.H.; Methodology − R.H., A.B., and V.R.K.; Investigation- R.H.; Writing original draft − R.H.; Writing review and editing − H.N., A.B., and B.R.R.K.; Software − R.H., G.B.H., and H.N.A.; Data curation − S.V.R., V.K., and K.S.D.; Supervision − K.S.D.; Validation − K.S.D., S.V.R., and A.B.; Formal analysis − H.N., R.A.A., H.N.A., and D.D.A.; Graphical abstract − R.H. and D.D.A.

Notes

The authors declare no competing financial interest.

■ ACKNOWLEDGMENTS

R.H., thankfully, acknowledges the Karnatak University Dharwad for the URS fellowship. the authors acknowledge Chromed Biosciences Private Limited, Tumkuru, India for providing the lab specialty to conduct the animal study, authors sincerely acknowledge the DFRL Mysore for providing the HPLC-ECD facility; authors acknowledge the Vipragen Biosciences Private Limited, Mysore, India for providing the LC-MS/MS specialty, authors sincerely acknowledge the USIC Karnatak University, Dharwad for providing the essential instrumentation services for characterization of Nanocomposite and the authors acknowledge the central research laboratory, SDM College of Medical Sciences and Hospital, Shri Dharmastala Manjunatheswara University, Dharwad, Karnataka for providing the lab specialty to conduct the in vitro cell line studies. This work is supported by Princess Nourah bint Abdulrahman University Researchers Supporting Project number (PNURSP2025R148), Princess Nourah bint Abdulrahman University, Riyadh, Saudi Arabia.

■ ABBREVIATIONS

PD,Parkinson's disease; SNCA,Synuclein Alpha; LD,Levodopa; PDENC,polymer-based drug encapsulated nanocomposite; PCL,Poly-ε-caprolactone; LD-PCL-PVA NC,Levodopa encapsulated Poly-ε-caprolactone nanocomposite; FDA,Food and Drug Administration; FTIR,Fourier-transform infrared spectroscopy; TGA,thermomechanical analysis; FE-SEM,field-emission scanning electron microscopy; HR-TEM,high-resolution transmission electron microscopy; NaOH,sodium hydroxide; EDC,1-ethyl-3-(3-(dimethylamino)propyl) carbodiimide; NHS,*N*-hydroxy succinimide; PVA,poly(vinyl alcohol); PDI,polydispersive index; DLS,dynamic light scattering technique; AUC,area under the curve; DPN,dopaminergic neurons; ROT,rotenone; TEA,triethylamine; HVA,homovanillic acid; DA,dopamine; EDTA,ethylenediaminetetraacetic acid; DCM,dichloromethane; DMSO,dimethyl sulfoxide; EE,encapsulation efficiency; PBS,phosphate buffer saline; ip,intraperitoneal; H&E,Hematoxylin and Eosin; MTT,3-(4,5-dimethylthiazol-2-yl)-2,5-diphenyltetrazolium bromide; DMEME,-Dulbecco's Modified Eagle Medium; FBS,fetal bovine serum

■ REFERENCES

(1) Dauer, W.; Przedborski, S. Parkinson's Disease. *Neuron* **2003**, *39* (6), 889−909.

(2) Pardo-Moreno, T.; García-Morales, V.; Suleiman-Martos, S.; Rivas-Domínguez, A.; Mohamed-Mohamed, H.; Ramos-Rodríguez, J. J.; Melguizo-Rodríguez, L.; González-Acedo, A. Current Treatments and New, Tentative Therapies for Parkinson's Disease. *Pharmaceutics* **2023**, *15* (3), 770.

(3) Damier, P.; Hirsch, E. C.; Agid, Y.; Graybiel, A. M. The Substantia Nigra of the Human Brain. *Brain* **1999**, *122* (8), 1437−1448.

(4) Das, R.; Paul, S.; Mourya, G. K.; Kumar, N.; Hussain, M. Recent Trends and Practices Toward Assessment and Rehabilitation of Neurodegenerative Disorders: Insights From Human Gait. *Front. Neurosci.* **2022**, *16*, No. 859298.

(5) Prajjwal, P.; Flores Sanga, H. S.; Acharya, K.; Tango, T.; John, J.; Rodriguez, R. S. C.; Dheyaa Marsool Marsool, M.; Sulaimanov, M.; Ahmed, A.; Hussin, O. A. Parkinson's Disease Updates: Addressing the Pathophysiology, Risk Factors, Genetics, Diagnosis, along with the Medical and Surgical Treatment. *Ann. Med. Surg.* **2023**, *85* (10), 4887−4902.

(6) Hanumanthappa, R.; Parthasarathy, A.; Heggannavar, G. B.; Pc, K.; Nanjaiah, H.; Kumbhar, R.; Devaraju, K. S. Recent Advances in Therapeutic Strategies for Alzheimer's and Parkinson's Disease Using Protein/Peptide Co-modified Polymer Nanoparticles. *Neuroprotection* **2024**, *2*, 255.

(7) Dudhipala, N.; Gorre, T. Neuroprotective Effect of Ropinirole Lipid Nanoparticles Enriched Hydrogel for Parkinson's Disease: In Vitro, Ex Vivo, Pharmacokinetic and Pharmacodynamic Evaluation. *Pharmaceutics* **2020**, *12* (5), 448.

(8) Hanumanthappa, R.; Venugopal, D. M.; P C, N.; Shaikh, A.; BM, S.; Heggannavar, G. B.; Patil, A. A.; Nanjaiah, H.; Suresh, D.; Kariduraganavar, M. Y.; Raghu, S. V.; Devaraju, K. S. Polyvinylpyrrolidone-Capped Copper Oxide Nanoparticles-Anchored Pramipexole Attenuates the Rotenone-Induced Phenotypes in a *Drosophila* Parkinson's Disease Model. *ACS Omega* **2023**, *8* (50), 47482−47495.

(9) Van Vliet, E. F.; Knol, M. J.; Schiffelers, R. M.; Caiazzo, M.; Fens, M. H. A. M. Levodopa-Loaded Nanoparticles for the Treatment of Parkinson's Disease. *J. Controlled Release* **2023**, *360*, 212−224.

(10) Jankovic, J.; Tan, E. K. Parkinson's Disease: Etiopathogenesis and Treatment. *J. Neurol. Neurosurg. Psychiatry* **2020**, *91* (8), 795−808.

(11) Stoker, T. B.; Barker, R. A. Recent Developments in the Treatment of Parkinson's Disease. *F1000Research* **2020**, *9*, 862.

(12) Vong, L. B.; Sato, Y.; Chonpathompikunlert, P.; Tanasawet, S.; Hutamekalin, P.; Nagasaki, Y. Self-Assembled Polydopamine Nanoparticles Improve Treatment in Parkinson's Disease Model Mice and Suppress Dopamine-Induced Dyskinesia. *Acta Biomater.* **2020**, *109*, 220−228.

(13) Qi, L.; Thomas, E.; White, S. H.; Smith, S. K.; Lee, C. A.; Wilson, L. R.; Sombers, L. A. Unmasking the Effects of L-DOPA on Rapid Dopamine Signaling with an Improved Approach for Nafion Coating Carbon-Fiber Microelectrodes. *Anal. Chem.* **2016**, *88* (16), 8129−8136.

(14) Foster, H. D.; Hoffer, A. The Two Faces of L-DOPA: Benefits and Adverse Side Effects in the Treatment of Encephalitis Lethargica, Parkinson's Disease, Multiple Sclerosis and Amyotrophic Lateral Sclerosis. *Med. Hypotheses* **2004**, *62* (2), 177−181.

(15) Ahmad, M. Z.; Sabri, A. H. B.; Anjani, Q. K.; Domínguez-Robles, J.; Abdul Latip, N.; Hamid, K. A. Design and Development of Levodopa Loaded Polymeric Nanoparticles for Intranasal Delivery. *Pharmaceuticals* **2022**, *15* (3), 370.

(16) Li, S.-D.; Huang, L. Pharmacokinetics and Biodistribution of Nanoparticles. *Mol. Pharmaceutics* **2008**, *5* (4), 496−504.

(17) Begines, B.; Ortiz, T.; Pérez-Aranda, M.; Martínez, G.; Merinero, M.; Argüelles-Arias, F.; Alcudia, A. Polymeric Nanoparticles for Drug Delivery: Recent Developments and Future Prospects. *Nanomaterials* **2020**, *10* (7), 1403.

(18) Pahuja, R.; Seth, K.; Shukla, A.; Shukla, R. K.; Bhatnagar, P.; Chauhan, L. K. S.; Saxena, P. N.; Arun, J.; Chaudhari, B. P.; Patel, D. K.; Singh, S. P.; Shukla, R.; Khanna, V. K.; Kumar, P.; Chaturvedi, R. K.; Gupta, K. C. Trans-Blood Brain Barrier Delivery of Dopamine-Loaded Nanoparticles Reverses Functional Deficits in Parkinsonian Rats. *ACS Nano* **2015**, *9* (5), 4850−4871.
(19) Aminu, N.; Audu, M. M.Polycaprolactone-Based Nanoparticles for Advanced Therapeutic Applications. In *Polymeric Nanosystems*; Elsevier: 2023; pp 37−84.
(20) Bartnikowski, M.; Dargaville, T. R.; Ivanovski, S.; Hutmacher, D. W. Degradation Mechanisms of Polycaprolactone in the Context of Chemistry. *Geometry and Environment. Prog. Polym. Sci.* **2019**, *96*, 1−20.
(21) Nguyen, L. T. B.; Odeleye, A. O. O.; Chui, C.; Baudequin, T.; Cui, Z.; Ye, H. Development of Thermo-Responsive Polycaprolactone Macrocarriers Conjugated with Poly (N-Isopropyl Acrylamide) for Cell Culture. *Sci. Rep.* **2019**, *9* (1), 3477.
(22) Alex, A. T.; Joseph, A.; Shavi, G.; Rao, J. V.; Udupa, N. Development and Evaluation of Carboplatin-Loaded PCL Nanoparticles for Intranasal Delivery. *Drug Delivery* **2016**, *23* (7), 2144−2153.
(23) Ahmed, F.; Discher, D. E. Self-Porating Polymersomes of PEG−PLA and PEG−PCL: Hydrolysis-Triggered Controlled Release Vesicles. *J. Controlled Release* **2004**, *96* (1), 37−53.
(24) Heggannavar, G. B.; Vijeth, S.; Kariduraganavar, M. Y. Preparation of Transferrin-Conjugated Poly-ε-Caprolactone Nanoparticles and Delivery of Paclitaxel to Treat Glioblastoma across Blood-Brain Barrier. *Emergent Mater.* **2019**, *2* (4), 463−474.
(25) Xin, H.; Jiang, X.; Gu, J.; Sha, X.; Chen, L.; Law, K.; Chen, Y.; Wang, X.; Jiang, Y.; Fang, X. Angiopep-Conjugated Poly (Ethylene Glycol)-Co-Poly(ε-Caprolactone) Nanoparticles as Dual-Targeting Drug Delivery System for Brain Glioma. *Biomaterials* **2011**, *32* (18), 4293−4305.
(26) Mundargi, R. C.; Srirangarajan, S.; Agnihotri, S. A.; Patil, S. A.; Ravindra, S.; Setty, S. B.; Aminabhavi, T. M. Development and Evaluation of Novel Biodegradable Microspheres Based on Poly (d, l-Lactide-Co-Glycolide) and Poly(ε-Caprolactone) for Controlled Delivery of Doxycycline in the Treatment of Human Periodontal Pocket. In Vitro and in Vivo Studies. *J. Controlled Release* **2007**, *119* (1), 59−68.
(27) Singh, E.; Osmani, R. A. M.; Banerjee, R.; Abu Lila, A. S.; Moin, A.; Almansour, K.; Arab, H. H.; Alotaibi, H. F.; Khafagy, E.-S. Poly ε-Caprolactone Nanoparticles for Sustained Intra-Articular Immune Modulation in Adjuvant-Induced Arthritis Rodent Model. *Pharmaceutics* **2022**, *14* (3), 519.
(28) Ammar, H. O.; Ghorab, M. M.; Mahmoud, A. A.; Higazy, I. M. Lamotrigine Loaded Poly-ε- (d, l-Lactide-Co-Caprolactone) Nanoparticles as Brain Delivery System. *Eur. J. Pharm. Sci.* **2018**, *115*, 77−87.
(29) Sawant, K.; Pandey, A.; Patel, S. Aripiprazole Loaded Poly(Caprolactone) Nanoparticles: Optimization and in Vivo Pharmacokinetics. *Mater. Sci. Eng., C* **2016**, *66*, 230−243.
(30) Mohamadpour, H.; Azadi, A.; Rostamizadeh, K.; Andalib, S.; Saghatchi Zanjani, M. R.; Hamidi, M. Preparation, Optimization, and Evaluation of Methoxy Poly (Ethylene Glycol)- *Co* -Poly(ε-Caprolactone) Nanoparticles Loaded by Rivastigmine for Brain Delivery. *ACS Chem. Neurosci.* **2020**, *11* (5), 783−795.
(31) Ortiz, R.; Cabeza, L.; Arias, J. L.; Melguizo, C.; Álvarez, P. J.; Vélez, C.; Clares, B.; Áranega, A.; Prados, J. Poly(Butylcyanoacrylate) and Poly(ε-Caprolactone) Nanoparticles Loaded with 5-Fluorouracil Increase the Cytotoxic Effect of the Drug in Experimental Colon Cancer. *AAPS J.* **2015**, *17* (4), 918−929.
(32) Kuo, Y.-C.; Chang, Y.-H.; Rajesh, R. Targeted Delivery of Etoposide, Carmustine and Doxorubicin to Human Glioblastoma Cells Using Methoxy Poly(Ethylene Glycol)-poly(E-caprolactone) Nanoparticles Conjugated with Wheat Germ Agglutinin and Folic Acid. *Mater. Sci. Eng., C* **2019**, *96*, 114−128.
(33) Jain, N.; Singh, V. K.; Chauhan, S. A Review on Mechanical and Water Absorption Properties of Polyvinyl Alcohol Based Composites/Films. *J. Mech. Behav. Mater.* **2017**, *26* (5−6), 213−222.
(34) Vera Garcia, P. F.; Guerrero Dimas, L. A.; Cedillo Portillo, J. J.; Martínez Anguiano, O. A.; Sáenz Galindo, A.; Narro Cespedes, R. I.; Acuña Vazquez, P.; Castañeda Facio, A. PVA Blends and Nanocomposites, Properties and Applications: A Review. In *Green-Based Nanocomposite Materials and Applications*; Avalos Belmontes, F.; González, F. J.; López-Manchado, M. Á., Eds.; Engineering Materials; Springer International Publishing: Cham, 2023; pp 191−206.
(35) Kayan, G. Ö.; Kayan, A. Polycaprolactone Composites/Blends and Their Applications Especially in Water Treatment. *ChemEngineering* **2023**, *7* (6), 104.
(36) Afzal, A.; Jalalah, M.; Noor, A.; Khaliq, Z.; Qadir, M. B.; Masood, R.; Nazir, A.; Ahmad, S.; Ahmad, F.; Irfan, M.; Afzal, M.; Faisal, M.; Alsareii, S. A.; Harraz, F. A. Development and Characterization of Drug Loaded PVA/PCL Fibres for Wound Dressing Applications. *Polymers* **2023**, *15* (6), 1355.
(37) Song, B.; Cho, C.-W. Applying Polyvinyl Alcohol to the Preparation of Various Nanoparticles. *J. Pharm. Investig.* **2024**, *54* (3), 249−266.
(38) Sahu, T.; Ratre, Y. K.; Chauhan, S.; Bhaskar, L. V. K. S.; Nair, M. P.; Verma, H. K. Nanotechnology Based Drug Delivery System: Current Strategies and Emerging Therapeutic Potential for Medical Science. *J. Drug Delivery Sci. Technol.* **2021**, *63*, No. 102487.
(39) Afzal, O.; Altamimi, A. S. A.; Nadeem, M. S.; Alzarea, S. I.; Almalki, W. H.; Tariq, A.; Mubeen, B.; Murtaza, B. N.; Iftikhar, S.; Riaz, N.; Kazmi, I. Nanoparticles in Drug Delivery: From History to Therapeutic Applications. *Nanomaterials* **2022**, *12* (24), 4494.
(40) Ball, V. Polydopamine Nanomaterials: Recent Advances in Synthesis Methods and Applications. *Front. Bioeng. Biotechnol.* **2018**, *6*, 109.
(41) Ekinci, M.; Yeğen, G.; Aksu, B.; İlem-Özdemir, D. Preparation and Evaluation of Poly (Lactic Acid)/Poly (Vinyl Alcohol) Nanoparticles Using the Quality by Design Approach. *ACS Omega* **2022**, *7* (38), 33793−33807.
(42) Farag, O. F.; Abdel-Fattah, E. Synthesis and Characterization PVA/Plasma-Functionalized MWCNTs Nanocomposites Films. *J. Polym. Res.* **2023**, *30* (5), 183.
(43) Ledeti, I.; Bolintineanu, S.; Vlase, G.; Circioban, D.; Ledeti, A.; Vlase, T.; Suta, L.-M.; Caunii, A.; Murariu, M. Compatibility Study between Antiparkinsonian Drug Levodopa and Excipients by FTIR Spectroscopy, X-Ray Diffraction and Thermal Analysis. *J. Therm. Anal. Calorim.* **2017**, *130* (1), 433−441.
(44) Zhou, Y. Z.; Alany, R. G.; Chuang, V.; Wen, J. Optimization of PLGA Nanoparticles Formulation Containing L-DOPA by Applying the Central Composite Design. *Drug Dev. Ind. Pharm.* **2013**, *39* (2), 321−330.
(45) Sardjono, R. E.; et al. Levodopa Nanoencapsulation in Nanostarch as Anti-Parkinsonian Drugs Candidate. *Indian J. Chem.* **2023**, *62* (10), 1056−1060.
(46) Nie, T.; He, Z.; Zhu, J.; Chen, K.; Howard, G. P.; Pacheco-Torres, J.; Minn, I.; Zhao, P.; Bhujwalla, Z. M.; Mao, H.-Q.; Liu, L.; Chen, Y. Non-Invasive Delivery of Levodopa-Loaded Nanoparticles to the Brain via Lymphatic Vasculature to Enhance Treatment of Parkinson's Disease. *Nano Res.* **2021**, *14* (8), 2749−2761.
(47) Lee, K. H.; Khan, F. N.; Cosby, L.; Yang, G.; Winter, J. O. Polymer Concentration Maximizes Encapsulation Efficiency in Electrohydrodynamic Mixing Nanoprecipitation. *Front. Nanotechnol.* **2021**, *3*, No. 719710.
(48) Totaro, K. A.; Liao, X.; Bhattacharya, K.; Finneman, J. I.; Sperry, J. B.; Massa, M. A.; Thorn, J.; Ho, S. V.; Pentelute, B. L. Systematic Investigation of EDC/sNHS-Mediated Bioconjugation Reactions for Carboxylated Peptide Substrates. *Bioconjugate Chem.* **2016**, *27* (4), 994−1004.
(49) Di Battista, V.; Hey-Hawkins, E. Development of Prodrugs for Treatment of Parkinson 's Disease: New Inorganic Scaffolds for Blood-Brain Barrier Permeation. *J. Pharm. Sci.* **2022**, *111* (5), 1262−1279.

https://doi.org/10.1021/acsomega.5c00691
ACS Omega 2025, 10, 19682−19696

(50) Hoon, M.; Petzer, J.; Viljoen, F.; Petzer, A. The Design and Evaluation of an L-Dopa−Lazabemide Prodrug for the Treatment of Parkinson's Disease. *Molecules* **2017**, *22* (12), 2076.
(51) Hörmann, P.; Delcambre, S.; Hanke, J.; Geffers, R.; Leist, M.; Hiller, K. Impairment of Neuronal Mitochondrial Function by L-DOPA in the Absence of Oxygen-Dependent Auto-Oxidation and Oxidative Cell Damage. *Cell Death Discovery* **2021**, *7* (1), 151.
(52) Ibarra-Gutiérrez, M. T.; Serrano-García, N.; Orozco-Ibarra, M. Rotenone-Induced Model of Parkinson's Disease: Beyond Mitochondrial Complex I Inhibition. *Mol. Neurobiol.* **2023**, *60* (4), 1929−1948.
(53) Rocha, S. M.; Bantle, C. M.; Aboellail, T.; Chatterjee, D.; Smeyne, R. J.; Tjalkens, R. B. Rotenone Induces Regionally Distinct α-Synuclein Protein Aggregation and Activation of Glia Prior to Loss of Dopaminergic Neurons in C57Bl/6 Mice. *Neurobiol. Dis.* **2022**, *167*, No. 105685.
(54) Niederberger, E.; Wilken-Schmitz, A.; Manderscheid, C.; Schreiber, Y.; Gurke, R.; Tegeder, I. Non-Reproducibility of Oral Rotenone as a Model for Parkinson's Disease in Mice. *Int. J. Mol. Sci.* **2022**, *23* (20), 12658.
(55) Bai, Q.; He, J.; Tang, Y.; Wang, S.; Qiu, J.; Wang, Y.; Yu, C. Rotenone-Induced Energy Stress Decompensated in Ventral Mesocerebrum Is Associated with Parkinsonism Progression in Rats. *Exp. Ther. Med.* **2016**, *12* (2), 1060−1066.
(56) Shi, X.; Bai, H.; Wang, J.; Wang, J.; Huang, L.; He, M.; Zheng, X.; Duan, Z.; Chen, D.; Zhang, J.; Chen, X.; Wang, J. Behavioral Assessment of Sensory, Motor, Emotion, and Cognition in Rodent Models of Intracerebral Hemorrhage. *Front. Neurol.* **2021**, *12*, No. 667511.
(57) Miyazaki, I.; Asanuma, M. The Rotenone Models Reproducing Central and Peripheral Features of Parkinson's Disease. *NeuroSci.* **2020**, *1* (1), 1−14.
(58) Troshev, D.; Voronkov, D.; Pavlova, A.; Abaimov, D.; Latanov, A.; Fedorova, T.; Berezhnoy, D. Time Course of Neurobehavioral Disruptions and Regional Brain Metabolism Changes in the Rotenone Mice Model of Parkinson's Disease. *Biomedicines* **2022**, *10* (2), 466.
(59) Khodir, S. A.; Sweed, E. M.; Faried, M. A.; Abo Elkhair, D. M.; Khalil, M. M.; Afifi, K. H.; El Agamy, D. F. Neuroprotective Effect of Maresin-1 in Rotenone-Induced Parkinson's Disease in Rats: The Putative Role of the JAK/STAT Pathway. *Neurochem. Res.* **2025**, *50* (1), 30.
(60) Mishra, A.; Singh, S.; Shukla, S. Physiological and Functional Basis of Dopamine Receptors and Their Role in Neurogenesis: Possible Implication for Parkinson's Disease. *J. Exp. Neurosci.* **2018**, *12*, No. 1179069518779829.
(61) Moussa, C. Dopamine Metabolite Biomarkers and Testing for Disease Modification in Parkinson Disease—Reply. *JAMA Neurol.* **2020**, *77* (8), 1039.
(62) Wang, T.; Li, C.; Han, B.; Wang, Z.; Meng, X.; Zhang, L.; He, J.; Fu, F. Neuroprotective Effects of Danshensu on Rotenone-Induced Parkinson's Disease Models in Vitro and in Vivo. *BMC Complement. Med. Ther.* **2020**, *20* (1), 20.
(63) Jenner, P.; Olanow, C. W. Oxidative Stress and the Pathogenesis of Parkinson's Disease. *Neurology* **1996**, *47*, S161.
(64) Guo, J.; Zhao, X.; Li, Y.; Li, G.; Liu, X. Damage to Dopaminergic Neurons by Oxidative Stress in Parkinson's Disease (Review). *Int. J. Mol. Med.* **2018**, *41*, 1817.
(65) Shahid Nadeem, M.; Khan, J. A.; Al-Abbasi, F. A.; AlGhamdi, S. A.; Alghamdi, A. M.; Sayyed, N.; Gupta, G.; Kazmi, I. Protective Effect of Hirsutidin against Rotenone-Induced Parkinsonism via Inhibition of Caspase-3/Interleukins-6 and 1β. *ACS Omega* **2023**, *8* (14), 13016−13025.
(66) Mbiydzenyuy, N. E.; Ninsiima, H. I.; Valladares, M. B.; Pieme, C. A. Zinc and Linoleic Acid Pre-Treatment Attenuates Biochemical and Histological Changes in the Midbrain of Rats with Rotenone-Induced Parkinsonism. *BMC Neurosci.* **2018**, *19* (1), 29.
(67) Akintunde, J. K.; Farai, T. I.; Arogundade, M. R.; Adeleke, J. T. Biogenic Zinc-Oxide Nanoparticles of Moringa Oleifera Leaves Abrogates Rotenone Induced Neuroendocrine Toxicity by Regulation of Oxidative Stress and Acetylcholinesterase Activity. *Biochem. Biophys. Rep.* **2021**, *26*, No. 100999.
(68) Lakshmi, Y.; Prasanth, D.; Kumar, K.; Ahmad, S.; Ramanjaneyulu, S.; Rahul, N.; Pasala, P. Unravelling the Molecular Mechanisms of a Quercetin Nanocrystal for Treating Potential Parkinson's Disease in a Rotenone Model: Supporting Evidence of Network Pharmacology and in Silico Data Analysis. *Biomedicines* **2023**, *11* (10), 2756.
(69) Smruthi, M. R.; Nallamuthu, I.; Anand, T. A Comparative Study of Optimized Naringenin Nanoformulations Using Nano-Carriers (PLA/PVA and Zein/Pectin) for Improvement of Bioavailability. *Food Chem.* **2022**, *369*, No. 130950.
(70) Ngwuluka, N. C.; Kotak, D. J.; Devarajan, P. V. Design and Characterization of Metformin-Loaded Solid Lipid Nanoparticles for Colon Cancer. *AAPS PharmSciTech* **2017**, *18* (2), 358−368.
(71) Luo, Z.; Zhao, Y.; Wang, Y.; Yang, X.; Zhao, B. Protective Effect of Theaflavins on Neuron against 6-Hydroxydopamine-Induced Apoptosis in SH-SY5Y Cells. *J. Clin. Biochem. Nutr.* **2012**, *50* (2), 133−138.
(72) Cheng, Q.; Chen, J.; Guo, H.; Lu, J.; Zhou, J.; Guo, X.; Shi, Y.; Zhang, Y.; Yu, S.; Zhang, Q.; Ding, F. Pyrroloquinoline Quinone Promotes Mitochondrial Biogenesis in Rotenone-Induced Parkinson's Disease Model via AMPK Activation. *Acta Pharmacol. Sin.* **2021**, *42* (5), 665−678.
(73) Ramachandra, V. H.; Sivanesan, S.; Koppal, A.; Anandakumar, S.; Howell, M. D.; Sukumar, E.; Vijayaraghavan, R. Embelin and Levodopa Combination Therapy for Improved Parkinson's Disease Treatment. *Transl. Neurosci.* **2022**, *13* (1), 145−162.
(74) Morais, L. H.; Lima, M. M. S.; Martynhak, B. J.; Santiago, R.; Takahashi, T. T.; Ariza, D.; Barbiero, J. K.; Andreatini, R.; Vital, M. A. B. F. Characterization of Motor, Depressive-like and Neurochemical Alterations Induced by a Short-Term Rotenone Administration. *Pharmacol. Rep.* **2012**, *64* (5), 1081−1090.
(75) Miyazaki, I.; Isooka, N.; Imafuku, F.; Sun, J.; Kikuoka, R.; Furukawa, C.; Asanuma, M. Chronic Systemic Exposure to Low-Dose Rotenone Induced Central and Peripheral Neuropathology and Motor Deficits in Mice: Reproducible Animal Model of Parkinson's Disease. *Int. J. Mol. Sci.* **2020**, *21* (9), 3254.
(76) Alabi, A. O.; Ajayi, A. M.; Ben-Azu, B.; Bakre, A. G.; Umukoro, S. Methyl Jasmonate Abrogates Rotenone-Induced Parkinsonian-like Symptoms through Inhibition of Oxidative Stress, Release of pro-Inflammatory Cytokines, and down-Regulation of Immnopositive Cells of NF-κB and α-Synuclein Expressions in Mice. *NeuroToxicology* **2019**, *74*, 172−183.
(77) Ozbey, G.; Nemutlu-Samur, D.; Parlak, H.; Yildirim, S.; Aslan, M.; Tanriover, G.; Agar, A. Metformin Protects Rotenone-Induced Dopaminergic Neurodegeneration by Reducing Lipid Peroxidation. *Pharmacol. Rep.* **2020**, *72* (5), 1397−1406.
(78) Singh, R.; Zahra, W.; Singh, S. S.; Birla, H.; Rathore, A. S.; Keshri, P. K.; Dilnashin, H.; Singh, S.; Singh, S. P. Oleuropein Confers Neuroprotection against Rotenone-Induced Model of Parkinson's Disease via BDNF/CREB/Akt Pathway. *Sci. Rep.* **2023**, *13* (1), 2452.
(79) Venkatesh Gobi, V.; Rajasankar, S.; Ramkumar, M.; Dhanalakshmi, C.; Manivasagam, T.; Justin Thenmozhi, A.; Essa, M. M.; Chidambaram, R.; Kalandar, A. *Agaricus Blazei* Extract Abrogates Rotenone-Induced Dopamine Depletion and Motor Deficits by Its Anti-Oxidative and Anti-Inflammatory Properties in Parkinsonic Mice. *Nutr. Neurosci.* **2018**, *21* (9), 657−666.
(80) Badawi, H.; Abdel-Salam, R.; Abdel-Salam, O.; Youness, E.; Shaffie, N.; Eldenshary, E. D. Bee Venom Attenuates Neurodegeneration and Motor Impairment and Modulates the Response to L-Dopa or Rasagiline in a Mice Model of Parkinson's Disease. *Iran. J. Basic Med. Sci.* **2020**, *23* (12), 1628−1638.
(81) El-Shamarka, M.; Abdel-Salam, O.; Shafee, N.; Zeidan, H. Curcumin Modulation of L-Dopa and Rasagiline-Induced Neuroprotection in Rotenone Model of Parkinson's Disease. *Iran. J. Basic Med. Sci.* **2023**, *26* (2), 139.

https://doi.org/10.1021/acsomega.5c00691
ACS Omega 2025, 10, 19682−19696

(82) Lowry, O. H.; Rosebrough, N. J.; Farr, A. L.; Randall, R. J. Protein Measurement with the Folin Phenol Reagent. *J. Biol. Chem.* **1951**, *193* (1), 265−275.
(83) Tabassum, A.; H, R.; K, J.; S, D.; M, B. The Prediction of Milk Whey Extract (MWE) Bioactive Compounds Based on Proximate Analysis and Its Effects on Blood Coagulation: A New Approach. *Curr. Res. Nutr. Food Sci. J.* **2024**, *12* (1), 437−451.
(84) Parthasarathy, A.; Hanumanthappa, R.; Bulbule, S. R.; Kiran, P. C.; Nanjaiah, H.; Gopinath, G.; Siddaiah, B. M.; Muniswamy, D.; Kuramkote Shivanna, D. Stress Enhances Expression of Calcium-binding Proteins and NMDAR Subunit Genes in the Rat Hippocampus. *Neuroprotection* **2024**, *2*, 167.
(85) Hanumegowda, S.; Srinivasa, C.; Shivaiah, A.; Venkatappa, M.; Hanumanthappa, R.; Rangappa, R.; Laxmaiah, R.; Gonchigar, S.; Sannaningaiah, D. Protein Extract of Kenaf Seed Exhibits Anticoagulant, Antiplatelet and Antioxidant Activities. *Asian Pac. J. Trop. Biomed.* **2022**, *12* (2), 47.

https://doi.org/10.1021/acsomega.5c00691
ACS Omega 2025, 10, 19682−19696